International Journal of Precision Engineering and Manufacturing (2024) 25:913–923
https://doi.org/10.1007/s12541-023-00948-8

Online ISSN 2005-4602
Print ISSN 2234-7593

REGULAR PAPER

A FE Model for the Efficient Simulation of the Thermo-Elastic Machine Tool Behavior

Christian Brecher[1] · Mathias Dehn[1] · Stephan Neus[1]

Received: 13 January 2023 / Revised: 13 December 2023 / Accepted: 14 December 2023 / Published online: 2 February 2024

Abstract
In modern machine tools, the thermo-elastic positioning error has a large share on the overall machine tool error. A multitude of different approaches can be found in the literature to correct this error in order to improve the accuracy of the machine tool. However, an FE-based approach to model the thermo-elastic error of 5 axis machine tools is still an active field of research. Therefore, the goal of this work is the improvement of the machine tool accuracy by modelling the machine tool error using a FE model. The model uses real time measurement data of the thermo-elastic error using an R-Test, as well as real time temperature measurements of the machine structure.

Keywords Thermal issues · Thermal error compensation · FE model · Machine tool error

1 Introduction

One of the defining criteria leading to a purchase decision is the productivity of the machine tool. Productivity is closely linked to machining quality [1]. When the machine tool productivity is increased, the heat generation in the machine rises as well. As a result of the higher heat generation, the deformation of the machine structure becomes larger and the Tool Center Point (TCP) displacement increases. The effect of the increased TCP displacement is a reduction in machining accuracy and as a result a reduced workpiece quality. Consequently, there is an increasing need for methods that can compensate or correct the TCP displacement.

✉ Mathias Dehn
M.Dehn@wzl.rwth-aachen.de

Christian Brecher
C.Brecher@wzl.rwth-aachen.de

Stephan Neus
S.Neus@wzl.rwth-aachen.de

[1] Laboratory for Machine Tools and Production Engineering (WZL) of RWTH Aachen University, Steinbachstr. 19, 52074 Aachen, Germany

2 Current Research

Since the thermo-elastic machine tool error can contribute a large share of the overall machine tool error, current research focuses on its computation, correction and compensation.

For an accurate estimation of the thermo-elastic TCP displacement, most of the research projects rely on measuring the thermo-elastic error [1]. In 5 axes machine tools, the thermo-elastic errors can usually not be measured fully using conventional measurement methods like laser interferometers, touch probes or measurement rulers. Therefore, indirect measurement methods using lasertracers or machining tests are used more often [2]. However, these measurement methods are time-consuming and can be expensive. A new approach of measuring the thermo-elastic machine error is described by Weikert and Bringmann et al. [3?5]. The approach focuses on a so-called ?R-Test?, using a calibration ball positioned on the machine table and a proximity sensor mounted into the spindle. The proximity sensor can measure the distance to the calibration ball during machine movement in all three directions of space. This measurement procedure was refined by Florussen and Brecher with the introduction of a dynamic R-Test [6, 7]. With this development, the measurement time to capture the machine tool errors was reduced, so that the measurement provides an accurate snapshot of the machine errors at a specific time.

In current research, the computation of the thermo-elastic error using FE models is becoming more and more

established for machine tool parts and assemblies, such as specific structural components [8], ball screws [9] or the spindle [10]. Modelling the complete machine tool on the other hand still comprises large difficulties. Due to the large physical size of machine tools and the large number of interacting parts and components, modelling the machine tools behavior is a complex task that requires large computing power. With the additional requirement of the model being capable of real time computing, emerges the need for even more computing power or an efficient model order reduction, as introduced by Vettermann et al. [11].

However, there are multiple research projects focussing on modelling the thermo-elastic TCP error for the complete machine tool without the requirement of real time computation. Maier uses a FE-based model to improve the machine design process [12]. During the design stage of a machine tool, real time computation is not necessary. Mayr uses the finite difference method to efficiently calculate the thermal field of the machine tool and a FE-based method to calculate the mechanical deformation and the TCP displacement [13]. By using model reduction methods, he achieves a fast computation time, making the model real time capable. Another method for a fast computation of the thermo-elastic machine tool error is introduced by Ess [14]. With the connection of FE simulation and ridged body elements, a quick computation is possible. However, due to the large degree of abstraction, the model was only able to compensate 50% of the thermo-elastic machine tool error. Beitelschmidt et al. discuss strategies and concepts for a FE based online simulation of the thermo-elastic error for the complete machine tool and apply their concept on a machine structure component [15]. They manage to reduce the simulation time drastically while not reducing the accuracy of the calculation compared to a traditional FE simulation using the Software ANSYS. However, they do not apply the model to a complete machine tool.

While Turek and Jungnickel discuss parts of the thermo-elastic error computation as well as the fundamental physical and mathematical functions, they do not apply the discussed work to a practical use case [16, 17]. A reason for this may be that the economically available computing power considered by Jungnickel and Turek was not large enough to accurately compute a FE model of a complete machine tool.

3 Methods

As shown above, it is not yet possible to compute the thermo-elastic machine tool error in thermal real time with a mesh that is fine enough, to deliver accurate results. To deal with this problem, the method presented in this paper focuses on increasing the degree of abstraction to reduce the computing time. As an effect of this, the accuracy of the computation will be reduced. The machine structure temperature is obtained using 32 thermal sensors.

The thermal information gained is used in the model to increase the computation accuracy of the thermal field to compensate for the reduced accuracy due to the high degree of abstraction. Furthermore, the thermo-elastic error is measured in periodic intervals using a dynamic R-Test to increase the accuracy of the thermo-elastic error model as introduced by Brecher et al. (compare Fig. 1) [18].

As shown in the figure, the model uncertainty is expected to increase over time, since the model degree of abstraction is high. In order to still receive a precise result for the computation of the thermo-elastic TCP-error, it is measured in regular intervals. The measurement result is then fed back into the FE model to improve the model accuracy.

The architecture of the model is shown in Fig. 2. Before modeling, system matrices need to be created and linked. This procedure is described in detail in Sect. 3.1. After this, the thermal model continuously computes the thermal field of the machine tool structure. The model uses temperature data from external temperature sensors, as well as control data, which is all data from the machine control, such as axis position, axis speed, or motor current [19]. The thermal model is described in Sect. 3.2 in more detail. Next, Sect. 3.3 describes the structural model, which computes the displacement field of the machine structure. The structural model uses the TCP displacement, which is measured using a dynamic R-Test, which is conducted in regular intervals. In the last step, the TCP displacement is derived from the displacement field of the structure. The computed TCP displacement can be used to correct the TCP position using the machine control.

The model architecture is based on the research introduced by Brecher et al. [10] in the collaborative research center funded by the German research foundation dealing with the thermo-energetic machine tool design (SFB/TR 96).

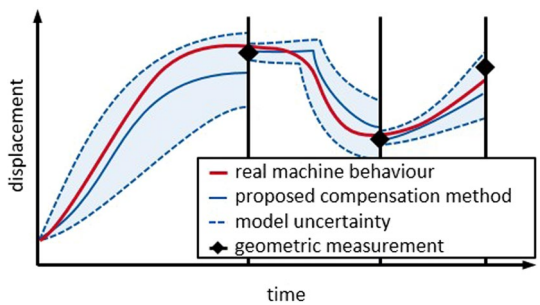

Fig. 1 Compensation method

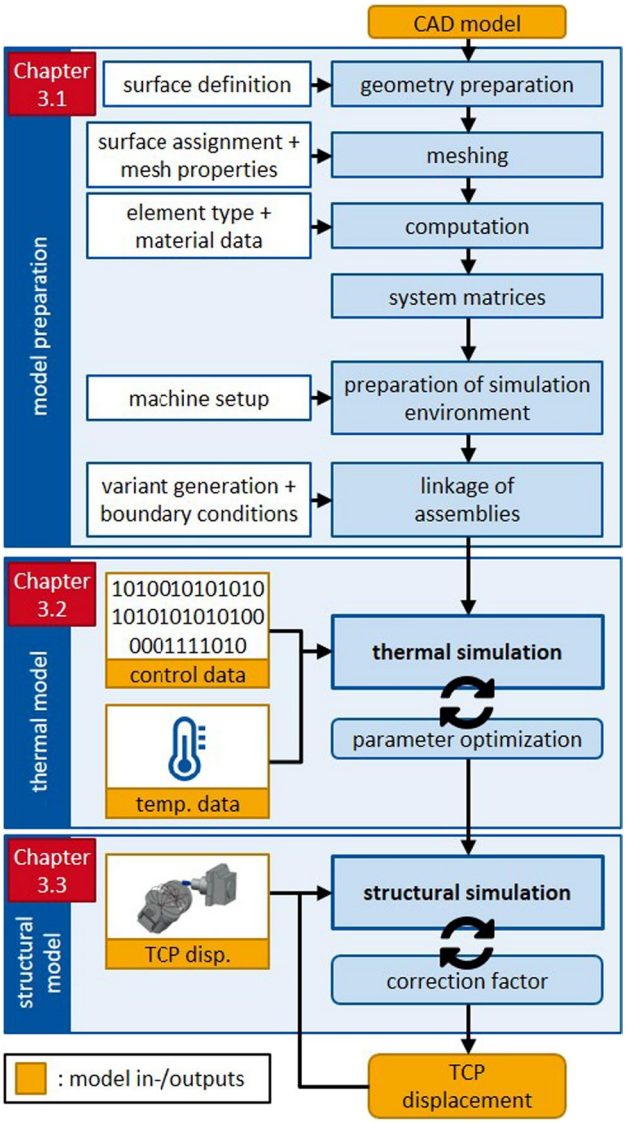

Fig. 2 FE model architecture

3.1 Model Preparation

Before the CAD model of the machine structure is processed in ANSYS, the CAD model degree of abstraction is defined. This is done by removing small features from the model. Next, the surfaces in contact with the environment are specified and the model is meshed in order to export the system matrices. The system matrices include the heat capacity, heat conduction and the mechanical stiffness matrix of the machine tool as well as the machine topology. Quadratic tetrahedron elements with four degrees of freedom per knot are used for meshing the machine tool structure. Tetraheron elements are commonly used when The degrees of freedom are their translational movement in the three directions in space and the temperature. Using rotational degrees of freedom would increase the number of degrees of freedom to a total of seven which drastically affects the computation time making the model unable of real time computation.

The system matrices are imported in MATLAB and prepared further for the simulation. The assemblies are linked in order to physically connect surfaces. There are two types of thermal linkages in the model. One is used for fixed contacts and one for moving contacts. Both of these are shown in Fig. 3.

For fixed contacts, the surfaces are meshed in a way, that there are the same number of nodes on both assembly surfaces with the same density, so the nodes can be connected one on one. For moving contacts, for example the contact between a guide rail and carriage, both surfaces are divided into segments. The segment contact temperature is set as the average temperature of all surface nodes of a segment.

The structural linkage of fixed contacts is conducted in the same manner as the thermal linkage of fixed contacts. Since the structural deformation of the machine is computed less frequently, its computation of the moving contacts can be more time-consuming, thus increasing the model accuracy. The contact method is shown in Fig. 4.

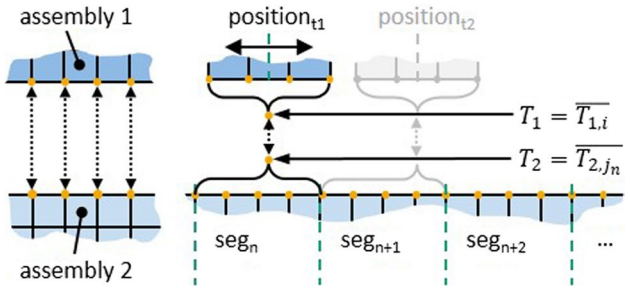

Fig. 3 Thermal linkage of machine parts for fixed (left) and moving (right) parts

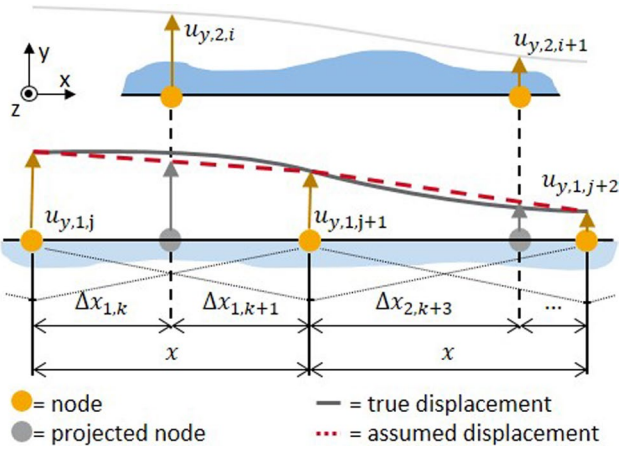

Fig. 4 Structural linkage of moving parts

In order to structurally link the parts, the displacement is interpolated at a projected position of the node of the counterpart. Equation (1) is used for the combined computation of the two parts.

$$w_{y,j} = \frac{x_i - \Delta x_i}{x_i} \cdot u_{y,i} + \frac{\Delta x_i}{x_i} \cdot u_{y,i+1} \tag{1}$$

where u_y = node displacement in Y-direction of assembly A, w_y = node displacement in Y-direction of assembly B, x = distance, i = node number in assembly A, j = node number in assembly B.

3.2 Thermal Model

The connected assemblies are used to compute the thermal field of the machine structure. The thermal model incorporates the following components:

- Natural convection for stationary and movable components
- Forced convection for movable components
- Friction heat from guides, bearings and ball screw nuts
- Heat from spindle and axis motors
- Heat flux within components
- Heat flux between components with fixed and moving contacts

The control data, as well as the temperature data gathered at 32 positions on the machine structure and the environment, is used to solve the fundamental transient equation for the thermal field (2) [10, 20].

$$\left[C_{th}\right]\left\{\dot{T}\right\} + \left[K_{th}\right]\{T\} = \left\{\dot{Q}\right\} \tag{2}$$

where $\left[C_{th}\right]$ = heat capacity matrix, $\left\{\dot{T}\right\}$ = temperature change vector, $\left[K_{th}\right]$ = heat conduction matrix, $\{T\}$ = temperature vector, $\left\{\dot{Q}\right\}$ heat vector.

The boundary conditions of the thermal system are defined in the heat conduction matrix.

$$\left\{\dot{Q}\right\} = \sum [B] \cdot [\dot{q}] \tag{3}$$

where $[B]$ = boundary condition matrix, $\left[\dot{q}\right]$ = heat density matrix of the boundary conditions.

The equation can only be solved numerically with time discretization. For this, a semi-implicit time integration method is used according to Eqs. (4) and (5)

$$\left\{\dot{T}\right\} = \frac{\left\{T_i - T_{i-1}\right\}}{\Delta t} \tag{4}$$

$$\{T\} = \{T_i\} \tag{5}$$

where T_i = temperature vector at time i, Δt = time step.

When combining the Eqs. (2)?(5), the following equation is formed:

$$\begin{aligned}([C_{th}] + \Delta t \cdot [K_{th}]) \cdot \left\{T_i\right\} =& [C_{th}] \cdot \left\{T_{i-1}\right\} \\ &+ \Delta t \cdot \sum ([B] \cdot [\dot{q}])\end{aligned} \tag{6}$$

To solve Eq. (6), the heat transfer is defined using control data. There are four areas, where the data is used to compute heat flux into and within the machine structure:

1. Definition of the contact position of moving axes using the respective axis positions according to Fig. 3.
2. Computation of the heat induced by the motors, using the respective motor current and a motor loss model.
3. Computation of the friction heat in the ball screw nuts and the guide rail [21] carriages using the respective axis speeds and a friction loss model
4. Computation of the forced convection of moving assemblies using the respective axis speed.

These computations of the heat flux are complex and subject to uncertainties and variation over time. A bottom up approach for the thermal model where each submodel is analytically described is a common approach in the Literature [12]. However, this approach is time-consuming regarding the implementation and it needs a large computing power, since it results in a large equation system. To reduce this effort, this paper focuses on a top-down approach for the thermal model. For the top-down modelling, the approach is to find a model that matches existing process parameters. A well known example for this is the use of neural networks, which are used to approximate a function that matches known input, to known output data [22]. Another example of the top-down approach, which is commonly used in the simulation of the thermo-elastic machine tool behavior, is the parametrization of low order delay elements based on measurement data, as done by Wennemer [2]. Similarly, in the work presented in this paper, the known temperature data is used to parametrize the functions describing the four kinds of heat fluxes listed above.

A top-down approach to modelling the thermo-elastic error with FE-modelling is used by Mares et al. [23]. In their work, they equip the machine with 70 temperature sensors and use thermal transfer functions to approximate the machine displacement. The coefficients in the thermal transfer function are determined by minimizing an error functioning consisting of measured and simulated temperatures. Mares approach is extended by Hojes et al. [24]. In an effort to validate the model, he was able to reduce the thermo-elastic error of a machine tool from a maximum of 75 µm to about 10 µm.

The same approach is used in this work, to integrate the data gathered from the temperature sensors into the FE

model. For this, an optimization parameter is introduced to the heat flux equations. The integration of this optimization parameter is shown for the convection heat flux (7) and the electric motor heat flux (8).

$$\dot{q}_{conv,i} = \alpha_{conv} \cdot (T_{k,i-1} - T_{E,i-1}) = R_{\alpha} \cdot (T_{k,i-1} - T_{E,i-1}) \quad (7)$$

where $\dot{q}_{conv}$ = heat flux density, R_{α} = optimization parameter, α_{conv} = surface heat transfer coefficient, T_k = temperature of node k, T_E = environment temperature, i = current time step.

$$\dot{q}_M = \frac{R_{R/s} \cdot I^2}{A_Q} = R_M \cdot I^2 \quad (8)$$

where $\dot{q}_M$ = motor heat flux, $R_{R/S}$ = total power resistance of the motor, I_m = motor current, A_Q = effective heat flux surface, R_M optimization parameter.

In Eq. (7), the convection heat flux is divided into a natural convection heat flux and a forced convection heat flux. The value of the natural convection coefficient is taken from the literature. The forced convection coefficient is assumed to be 0 for stationary components. For movable components, it is converted into an optimization parameter. Since the temperatures of the part and the environment are known for the previous time step, the heat flux can be computed after the optimization parameter is defined.

To simplify the thermal model, it is assumed, that the heat generated in the motor is formed similar to a resistor with the total power resistance of the motor. To receive the heat flux, the effective heat flux surface is taken into account. The equation is then simplified.

In order to calculate the optimization parameters, the before mentioned top done approach is used. This is done with an optimization function shown in Fig. 5.

Literature values for the optimization parameters vary largely. The convection coefficient for example depends on many boundary conditions like the surface condition, part geometry or wind speed. To solve the equation without knowing the value of the heat transfer coefficient, the thermal sensors are used. For a defined time period, the measured temperatures and the simulated temperatures at the sensor positions are compared by forming an error function. The optimization parameters are then adjusted within their physical limitations, so the error function is minimal. The optimization procedure is stopped, when a minimum is reached or the number of iterations surpasses a predefined maximum. The second stop criterion is implemented, to ensure that the computation time is limited. The same optimization factor is introduced for the friction losses in the ball screw nut and guide rails.

3.3 Structural Model

The structural model is prepared for 125 predefined machine poses. These machine poses are all combinations of equidistant positions of the linear axes X, Y and Z. The structural simulation computes the displacement field of the machine structure and the resulting TCP displacement for these poses. Machine poses in between these finite positions can be obtained using 3D interpolation. The procedure of determining the volumetric TCP displacement in the workspace is shown in Fig. 6.

For both sides of the kinematic chain, the surrounding nodes of the point of interest are analyzed to determine the tilt of the plane. Using the tilt angle of the plane, the point of interest is projected into the working volume. The machine pose is set so that an intersection between the theoretical workpiece and TCP is reached.

Every FE model has a computation error leading. Since the degree of abstraction is chosen quite high to enable an online correction, a larger computation error is expected.

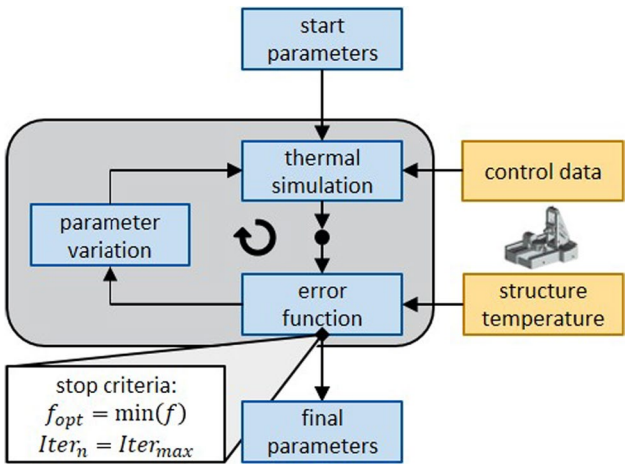

Fig. 5 Optimization function to determine thermal model parameters

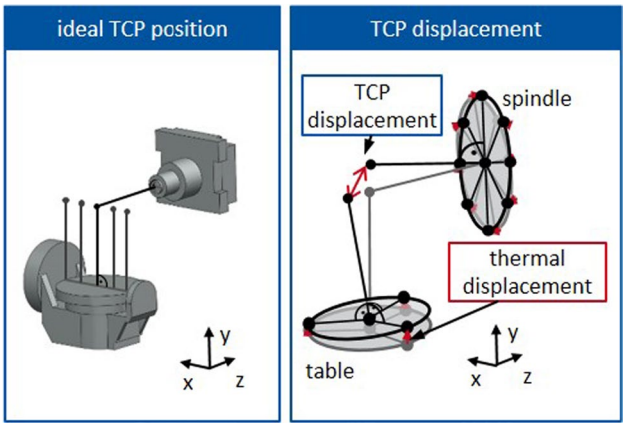

Fig. 6 Schematic depiction of the TCP displacement in the workspace

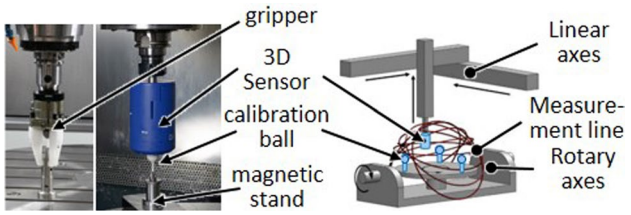

Fig. 7 Sketch of the dynamic R-Test and calibration ball placement according to [6]

To reduce the error of the structural model, it uses TCP displacement error measurements to align the computation with reality. In this case, a dynamic R-Test is used for this [6]. Figure 7 shows a sketch of the dynamic R-Test measurement procedure.

To conduct this test, a gripper, which holds a calibration ball mounted on a magnetic stand, is stored in the tool changer. After the tool is put in the spindle, it places the calibration ball eccentrically on the table. The now empty gripper is exchanged for a 3D-Probe. The 3D-Probe continuously measures the position of the previously placed calibration ball in the three spatial dimensions. The calibration ball conducts several circular movements by turning both rotary axes. To improve the measurement accuracy, the position of the calibration ball on the table is changed using the gripper, and the measurement is repeated. Using the continuous measurement results, the single axis errors defined in ISO 230-1 [25] are computed. The computation is conducted according to Brecher et al. by modeling the calibration ball position using the machine tool with homogeneous transformation matrices (HTM), which contain the single axis errors [6].

$$P_{ball} = T_t^{-1} \cdot T_w \tag{9}$$

where P_{ball} = measured ball position, T_t = transformation matrix of the tool sided axes, T_w = transformation matrix of the workpiece sided axes.

By solving Eq. (9), 15 out of the 21 single axis errors of the linear kinematic are obtained. Due to the flexible positioning of the calibration ball using the gripper, and the ability to place it at will, the measurement system is not limited by workpieces that are manufactured on the machine.

4 Validation and Discussion

To investigate the behavior of the structural model, the machine is put under varying loads. In this paper, the results for an X-axis load are investigated in more detail. In the first 4 h of the experiment, the X-axis is moved back and forth at a constant speed. Therefore, the X-axis current is elevated. After 4 h of thermal load, the machine is stopped, which lowers the X-axis current. It can also be seen, that the Y-axis current is constantly elevated throughout the duration of the experiment. Since the Y-axis is the vertical axis of the machine, it needs to apply a constant torque in order to counteract gravity, resulting in a higher torque. The spikes in the graph can be contributed to the R-Test. During the first 4 h, an R-Test measurement is conducted every hour in order to measure the thermal error of the machine. After this, during cool down, the measurement frequency is lowered to once every 2 h to induce less heat during this cool down phase.

All experiments are conducted on a five axes machining center with a horizontal spindle. The created model is used to investigate the machine tool behavior. First, the simulated thermal field of the machine structure is investigated. Figure 8 shows the simulated and measured machine structure temperature at three positions along the X-axis. In this setup, the machine is put under load by constantly moving the X-axis for 4 h. After this, the machine is stopped for a cool down. Furthermore, the difference between the measured and simulated temperature is evaluated.

For the plotted temperatures, the simulation is an acceptable approximation of the measured values. It can be seen that the error between the measured and the simulated temperature reaches a maximum of 1.5 °C. This maximum deviation occurs at the sensor position close to the X-axis motor around the 4 h mark, where the load changes. This is an indication, that the thermal model shows larger error when the loads are changing drastically. A repeated quick temperature change can be observed during the R-Test measurements, e.g. Fig. 8 Mark 1. The R-Tests leads to a change of heat induced in the machine tool. While the simulation approximates the real measurements well during the heat up phase,

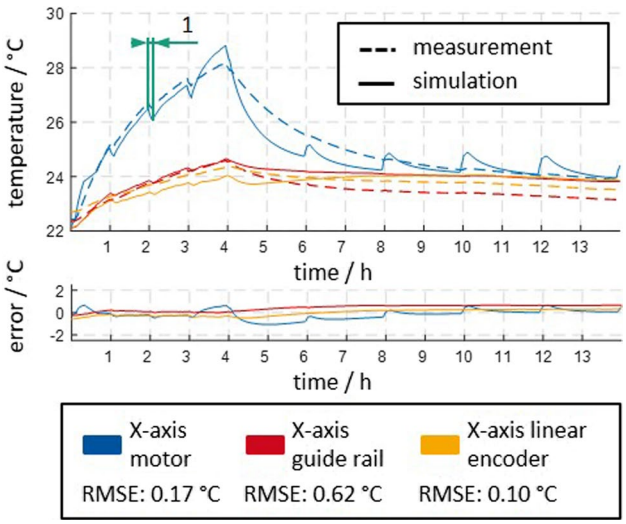

Fig. 8 Simulated and measured temperatures along the X-axis for an X-axis load

during cool down, the heat generated during the R-Test is slightly overestimated by the simulation. A reason for the occurring differences between measurement and simulation could be the high degree of abstraction chosen for the model. The simulated and measured temperature is also evaluated for three positions along the Y-axis and depicted in Fig. 9.

Similar to the three previously discussed results of the thermal field, the sensors on the positions along the Y-axis also show a low deviation from the simulated results, with a maximum error of 1.5 °C. Here, the same changes in heat flux can be observed at the time points where the R-Test measurement is conducted. It is striking, how the temperature of the Y-axis structure rises continuously for several hours after the machine is stopped. This can be attributed to the axes setup. The Y-axis is the vertical axis that needs to counteract gravity and apply torque. As a result, there is a heat flux into the machine tool structure even when the machine is not moving. It is noticeable, that the machine structure temperature is falling at the Y-axis motor when an R-Test is conducted. This is counterintuitive, since a movement during the R-Test should generate increased heat flux into the machine structure.

However, the effect of an increased forced convection due to the moving machine parts is dominant in this case, leading to a net heat loss close to the Y-axis motor resulting in a slight drop in temperature. Figure 10 shows the thermal field of the machine tool for multiple times during the experiment.

The thermal field of the machine tool is consistent with the previously shown figures. Figure 10 shows, that the maximum machine structure temperature occurs at the top of the Y-axis close to the Y-axis motor. The X-Axis motor shows the highest temperature at t = 4 h when the load is stopped. It is notable, that the high temperature areas of the machine tool are not incorporated in the kinematic chain of the machine tool and should therefore have a small impact on the TCP positioning error.

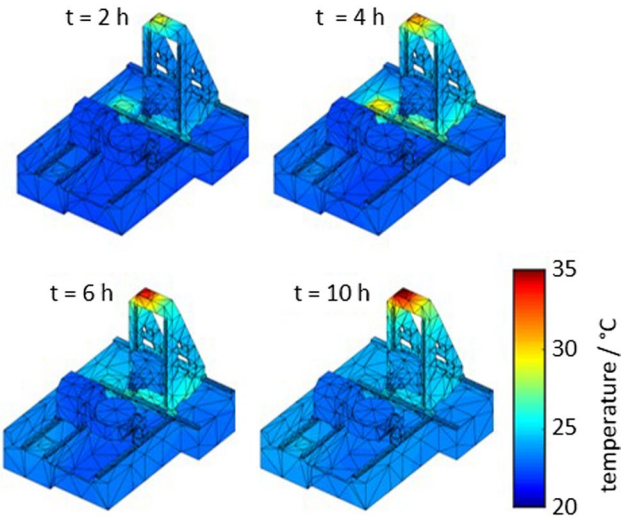

Fig. 10 Thermal field of the machine tool surface for four time points

Based on the thermal field of the machine tool structure, the displacement field is calculated as described in Chapter 3. The displacement field is shown in Fig. 11.

For each node, the total displacement from its initial position at time t = 0 h is computed and plotted. It can be seen, that the displacement field of the machine structure correlates with the thermal field shown in Fig. 9. Areas with a high temperature also show a large displacement. In particular, the Y-axis structure shows a large displacement of up to 100 µm. More interesting than the displacement of

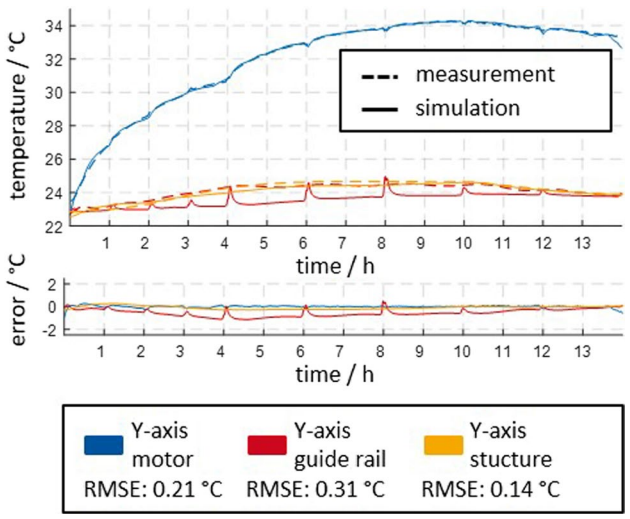

Fig. 9 Simulated and measured temperatures along the Y-axis for an X-axis load

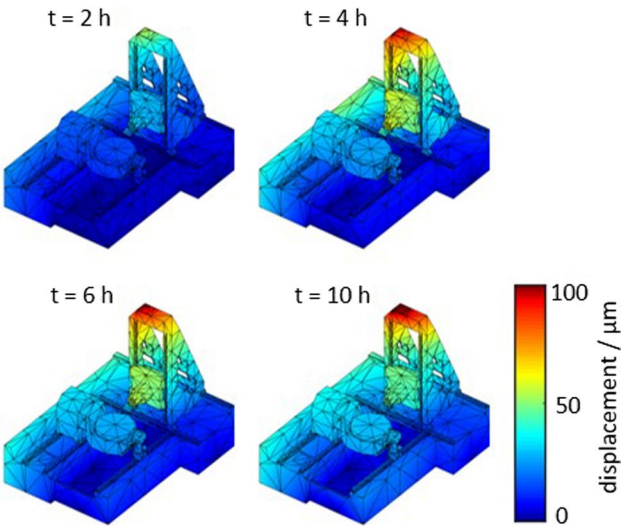

Fig. 11 Displacement field of the machine tool surface for four time points

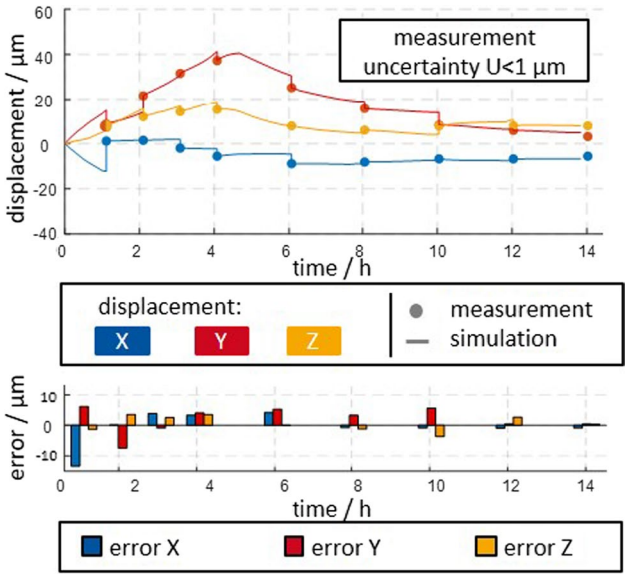

Fig. 12 Simulated and measured relative displacement between the machine tool table and spindle under internal load

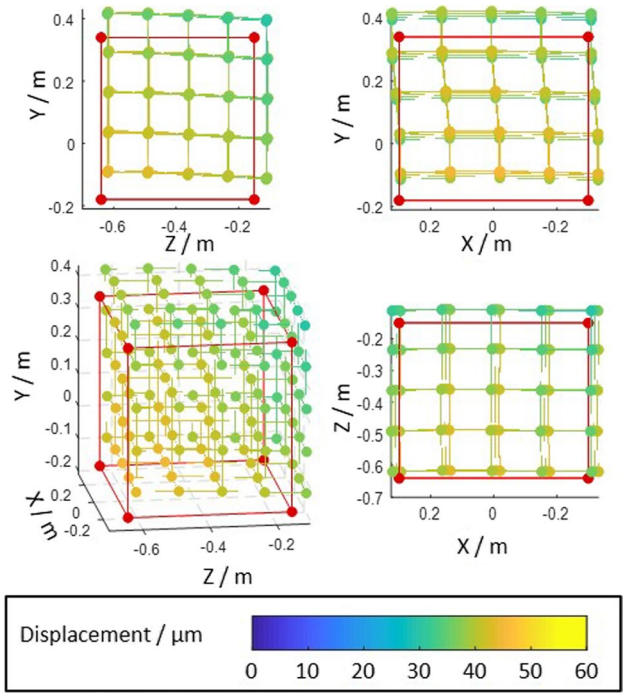

Fig. 13 Volumetric machine tool error in the machine working volume

the machine structure is the relative displacement between the machine tool table and the spindle center. This relative displacement is evaluated in Fig. 12.

Figure 12 shows the relative displacement between the machine tool table and the spindle in the three spatial dimensions. Contrary to the thermal simulation, there is no continuous measurement of the machine displacement available. The displacement is only available at the discrete time points, where the R-Test is conducted. Only at these time points, an evaluation of the model error can be completed. The maximum model error amounts to up to 7 µm at the Y-axis at t = 10 h when the start of the experiment is not considered, since the model correction factor is not settled here. With a maximum measured error in the Y-axis of 38 µm, the model computes approximately 84% of the thermo-elastic machine error at this point. At the time points, where the measured displacement is lower, the model error is still approximately 7 µm and therefore constitutes a higher share of the total displacement. Here, the model can compute 59% of the thermo-elastic error.

Since the model computes the error in the complete machine working volume, the volumetric machine error can be examined. Figure 13 shows the volumetric error in the machine working space after 4 h of internal thermal load. The reference volume is shown in red. The distortion is scaled up in order to make the form visible.

It can be seen, that the error consists mostly of a shift of the working volume. The distortion of the volume itself is comparatively small. Since the shift of the working volume can be detected using fewer machine poses, the number of poses calculated by the model may be reduced, thus improving the computation time of the model significantly without reducing its accuracy. However, a prerequisite for this reduction of calculated machine poses is a more in depth analysis of the distortion of the working volume under multiple different load scenarios in order to ensure that the working volume shift is the dominating factor in all cases.

As described previously, the external influences on the machine can also be evaluated with the machine model. To investigate the accuracy of modelling the thermal machine error under external loads, an experiment is conducted. Here, the machine is first put under constant internal load for 7 h. Four hours after the experiment is started, the shop floor door is opened for 2 h, thus reducing the environment temperature. Afterwards, the machine is stopped and the model behavior during cooldown is observed. The result of this experiment is shown in Fig. 14.

The result of the machine displacement under external load shows, that the model is able to reduce the overall machine error also under external load scenarios. The maximum measured error using the R-Test amounts to 48 µm in Y-direction. At this point, the model computes an error of 35 µm, thus reducing the machine error by 72%. However, it can be seen, that the largest model error occurs during and right after the external load is applied. Under the external load, the relevant physical parameters, as for example air temperature and airspeed change quickly. This results in a change in the heat transfer coefficient of the machine structure. This corresponds with investigations by

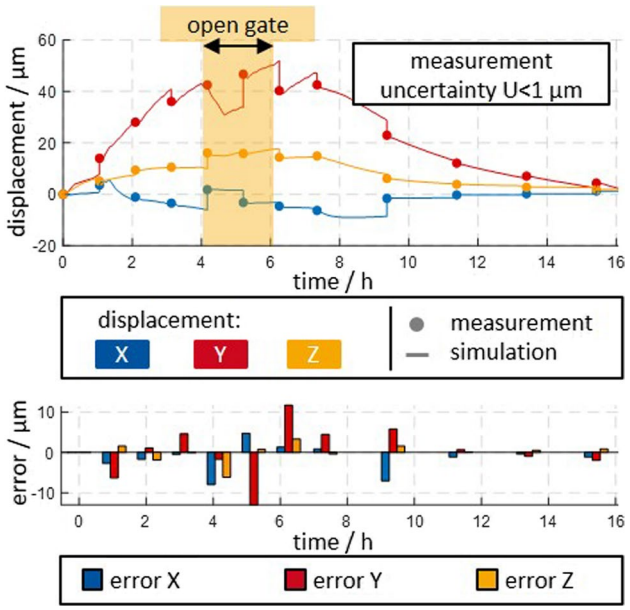

Fig. 14 Simulated and measured relative displacement between the machine tool table and spindle under internal and external load

Brecher et al. who find, that the heat transfer coefficients are highly dependent on these factors [26]. The model is not fast enough in changing corresponding coefficients to replicate the reality. Therefore, the model error is highest after the load is applied to and relived from the machine.

To compensate the machine error in real time, it is necessary to compute the machine error in real time. The main requirement for this is the computation of the TCP displacement in a defined time interval takes less time than the duration of the interval. The computation time of the thermal field of the machine is 0.015 s per time step of 1 min. Computing the displacement field of the machine structure on the other hand is more time-consuming with a computation time of 0.16 s per machine pose, resulting in a computation time of 20 s for 125 machine poses. In addition to this, a matrix decomposition has to be computed for each pose, which takes 2 s per pose. When using a computer with a large enough RAM (min. 64 GB), this decomposition can be computed once per machine pose before the simulation is started. Then it is stored in the RAM for the duration of the simulation and available for computations. With a smaller RAM (32 GB or less), the decomposition cannot be stored and has to be repeated once per machine pose for each computation of the displacement field, thus adding 250 s to the simulation time. Since this time is too long to be considered real time capable, the number of machine poses to be calculated must be reduced, to regain real time capability on a low-RAM computer. Under the constraint of real time capability on a low-RAM computer, up to 27 machine poses can be computed (three poses per direction).

Since the time constants of thermo-elastic TCP displacement are high, it is not necessary, that the thermo-elastic error is computed for each 1 min time step. The available time in the time steps where no computation of the displacement field is conducted is used to conduct the optimization of the thermal parameters, as shown in Fig. 2.

5 Summary and Outlook

In this paper, a FE method is presented, that can be used to quantify the thermo-elastic TCP error of a machine tool. The model successfully incorporates online machine data, online temperature measurements and online TCP measurements. The goal of reducing the models? degree of abstraction to be able to compute the machine errors in thermal real time was successful. A computation time of 20.9 s for a time period of 1 min with 125 machine poses on a high RAM computer and a computation time of 59.2 s for 27 machine poses on a low ram computer for the same simulation time of 1 min could be reached.

Under the incorporation of the real time measurement data from the machine, the model delivers satisfactory results. The model is able to compute the thermo-elastic machine error with an accuracy of at least 59% in the investigated load scenarios. However, the model shows weaknesses under abruptly changing loads. Furthermore, the model accuracy is strongly dependent on the measurement frequency of the machine geometry. The longer the measurement interval gets, the higher is the expected uncertainty of the computation. In this paper, a measurement frequency of once per hour was used during machine warm-up. This may not be economical for individual production processes, since the measurements cause a production interruption of about 5 min.

Therefore, the model should be refined before it is used in production. In order to increase the model accuracy and the robustness against abrupt load changes, it is necessary, that the model degree of abstraction is reduced. For this, faster computers need to be used in order for the model to be still real time capable. Since computers get increasingly faster with time, the feasibility of modelling the thermo-elastic error using a FE model should be reevaluated in a few years and model order reduction methods should be explored. At the moment however, it does not seem that the computation power available on standard computers is large enough for the FE based computation and compensation of the thermo-elastic error in real time.

Acknowledgements The presented findings are funded by the German Research Foundation (DFG, German Research Foundation)?Project ID 174223256?TRR 96.

Funding Open Access funding enabled and organized by Projekt DEAL.

References

1. Großmann, ed. (2015). Thermo-energetic design of machine tools. Lecture notes in production engineering. Cham: Springer. https://doi.org/10.1007/978-3-319-12625-8.
2. Wennemer, M. (2018). *Methode zur Messtechnischen Analyse und Charakterisierung Volumetrischer Thermo-elastischer Verlagerungen Von Werkzeugmaschienen*. Aachen: Apprimus Verlag.
3. Bringmann, B., & Knapp, W. (2006). Model-based ?chase-the-ball?? calibration of a 5-axes machining center. *CIRP Annals, 55*(1), 531?534. https://doi.org/10.1016/S0007-8506(07)60475-2
4. Bringmann, B., Küng, A., & Knapp, W. (2005). A measuring artefact for true 3d machine testing and calibration. *CIRP Annals, 54*(1), 471?474. https://doi.org/10.1016/S0007-8506(07)60147-4
5. Weikert, S. (2004). R-test, a new device for accuracy measurements on five axis machine tools. *CIRP Annals, 53*(1), 429?432. https://doi.org/10.1016/S0007-8506(07)60732-X
6. Brecher, C., Behrens, J., Lee, T. H., & Charlier, S. (2017). Calibration of five-axis machine tool using r-test procedure. Laser metrology and machine performance XII.
7. Florussen, G. H. J., & Spaan, H. A. M. (2012). Dynamic r-test for rotary tables on 5-axes machine tools. *Procedia CIRP, 1*, 536?539. https://doi.org/10.1016/j.procir.2012.04.095
8. Galant, A., Beitelschmidt, M., & Großmann, K. (2016). Fast high-resolution FE-based simulation of thermo-elastic behaviour of machine tool structures. *Procedia CIRP, 46*, 627?630. https://doi.org/10.1016/j.procir.2016.04.020
9. Thiem, X., Kauschinger, B., & Ihlenfeldt, S. (2017). Structure model based correction of thermally induced motion errors of machine tools. *Procedia Manufacturing, 14*, 128?135. https://doi.org/10.1016/j.promfg.2017.11.015
10. Brecher, C., Ihlenfeldt, S., Neus, S., Steinert, A., & Galant, A. (2019). Thermal condition monitoring of a motorized milling spindle. *Production Engineering, 13*(5), 539?546. https://doi.org/10.1007/s11740-019-00905-3
11. Vettermann, J., Steinert, A., Brecher, C., Benner, P., & Saak, J. (2022). Compact thermo-mechanical models for the fast simulation of machine tools with nonlinear component behavior. *Automatisierungstechnik, 70*(8), 692?704. https://doi.org/10.1515/auto-2022-0029
12. Maier, T. (2015). Modellierungssystematik zur Aufgabenbasierten Beschreibung des Thermoelastischen Verhaltens Von Werkzeugmaschinen: Dissertation. Forschungsberichte IWB, vol. 317. Herbert Utz Verlag, München
13. Mayr, J. (2009). Beurteilung und kompensation des temperaturganges von werkzeugmaschinen. Ph.D. thesis, ETH Zurich. https://doi.org/10.3929/ETHZ-A-006078492.
14. Ess, M. (2012). Simulation and compensation of thermal errors of machine tools. Ph.D. thesis, ETH Zurich. https://doi.org/10.3929/ETHZ-A-7357121.
15. Beitelschmidt, M., Galant, A., & Kauschinger, B. (2017). FE-basierte, Thermo-elastische online-Simulation Einer Gesamten WZM. Strategien, Konzepte und Workflow. TU Dresden SFB/TR 96, Dresden.
16. Jungnickel, D. (2000). Simulation des Thermischen Verhaltens Von Werkzeugmaschinen.
17. Turek, P., Jedrzejwski, J., & Modrzycki, W. (2010). Methods of machine tool error compensation. *Journal of Machine Engineering, 10*, 5?25.
18. Brecher, C., Neus, S., & Dehn, M. (2020). Efficient FE-modelling of the transient thermo-elastic machine behaviour of 5-axes machine tools thermal issues proceedings cover 2020. Special Interest Group Meeting: Thermal Issues: Laboratory for Machine Tools and Production Engineering (WZL) of RWTH Aachen, and Fraunhofer Institute for Production Technology IPT, DE, 26th ? 27th February 2020, Aachen/ Germany, 148?149.
19. Yoon, J.-S., Kim, Y.-D., Lee, J., & Lee, D. Y. (2023). Opc UA-based machining cell monitoring system for multi-vendors? machine tools and industrial robots. *International Journal of Precision Engineering and Manufacturing-Smart Technology, 1*(1), 63?69. https://doi.org/10.57062/ijpem-st.2022.0024
20. Nithiarasu, P., Lewis, R. W., & Seetharamu, K. N. (2016). *Fundamentals of the finite element method for heat and mass transfer* (2nd ed.). New Delhi: Wiley.
21. Sim, B., & Lee, W. (2023). Digital twin based machining condition optimization for CNC machining center. *International Journal of Precision Engineering and Manufacturing-Smart Technology, 1*(2), 115?123. https://doi.org/10.57062/ijpem-st.2023.0010
22. Aggarwal, C. C. (2018). *Neural networks and deep learning*. Cham: Springer. https://doi.org/10.1007/978-3-319-94463-0
23. Mares, M., Horejs, O., Hornych, J., & Smolik, J. (2013). Robustness and portability of machine tool thermal error compensation model based on control of participating thermal sources. *Journal of Machine Engineering, 13*, 24?36.
24. Horejs, O., Mares, M., & Hornych, J. (2013). Complex verification of thermal error compensation model of a portal milling centre. In *Proceedings of the international conference on advanced manufacturing engineering and technololgies* (pp. 233?242).
25. International Organization for Standardization: Test code for machine tools: Geometric accuracy of machines operating under no-load or quasi-static conditions (2012).
26. Brecher, C., Kneer, R., Spierling, R., Frekers, Y., & Fey, M. (2018). Ein beitrag zur modellierung des thermischen umgebungseinflusses an werkzeugmaschinen. *ZWF Zeitschrift für wirtschaftlichen Fabrikbetrieb, 113*, 1?5. https://doi.org/10.3139/104.111941

Prof. Dr.-Ing. Christian Brecher obtained his PhD from RWTH Aachen University in 2002. Currently, he holds the Chair of Machine Tools at RWTH Aachen University and is a board member at WZL and Fraunhofer IPT. His expertise spans academia and industry, focusing on advancing machine tools and manufacturing technologies.

Dipl.-Ing. Stephan Neus received a diploma in engineering in 2014 from RWTH Aachen University. Currently, he is a chief engineer and head of the department of Machine Technology at the WZL, RWTH Aachen University.

Mathias Dehn M. Sc., M. Sc. received a master's degree from RWTH Aachen and Tsinghua University. Currently, he is a research assistant at the WZL, RWTH Aachen University. His main research focus is the thermo-elastic behavior of machine tools.